GA–A27160

COMPARING PALEOCLASSICAL-BASED PEDESTAL MODEL PREDICTIONS OF ELECTRON QUANTITIES TO MEASURED DIII-D H-MODE PROFILES

by
S.P. SMITH, J.D. CALLEN, R.J. GROEBNER, T.H. OSBORNE,
A.W. LEONARD, D. ELDON, B.D. BRAY and THE DIII-D TEAM

DECEMBER 2011

GENERAL ATOMICS

DISCLAIMER

GA–A27160

COMPARING PALEOCLASSICAL-BASED PEDESTAL MODEL PREDICTIONS OF ELECTRON QUANTITIES TO MEASURED DIII-D H-MODE PROFILES

by
S.P. SMITH, J.D. CALLEN,* R.J. GROEBNER, T.H. OSBORNE,
A.W. LEONARD, D. ELDON,† B.D. BRAY and THE DIII-D TEAM

This is a preprint of a paper to be presented at the 13th International Workshop on H-mode Physics and Transport Barriers, October 10–12, 2011 in Oxford, United Kingdom and to be published in Nuclear Fusion.

*University of Wisconsin, Madison, Wisconsin USA
†University of California-San Diego, La Jolla, California USA

Work supported in part by
the U.S. Department of Energy
under DE-FC02-04ER54698
and DE-FG02-92ER54139

GENERAL ATOMICS PROJECT 30200
DECEMBER 2011

ABSTRACT

Accurately predicting the pedestal structure in high-(H-)confinement mode plasmas is of great importance for the modelling of future tokamak plasmas. The main predictions of a model of pedestal structure based on paleoclassical transport as the main transport mechanism are presented. Numerical evaluations of this model are compared with a database of measured DIII-D H-mode pedestal profiles. Across the database, the electron temperature gradient is overpredicted by a factor of 1.7 ± 1.1 and the electron density by a factor of 2.1 ± 0.7. These results are consistent with paleoclassical transport producing the minimum level of electron transport. Trends in the predictions indicate that some additional transport may be operative, especially in high β_{p} and low confinement plasmas.

1. INTRODUCTION

The regime in which the tokamak has found the greatest performance is the H-mode (high performance plasma confinement mode), which is characterized by an edge transport barrier that creates a pedestal in the edge electron density and temperature. The characteristics of the pedestal are extremely important because they serve as a boundary condition for the core of the plasma, and a sufficiently high pedestal pressure will be required to produce the desired fusion output in a burning plasma device.[1] To date, the EPED model has been fairly successful in predicting the height and width of the pressure pedestal just before an edge localized mode (ELM) by combining peeling-ballooning mode and kinetic ballooning mode constraints.[2] However, the individual constituents of the pressure are not resolved in the EPED model, nor is the time evolution between ELMs predicted. For these, one must have a transport solver that can individually evolve the density and temperature using experimentally validated transport models and processes. One of the difficult aspects of validating transport models is designing experiments that test the model in specific ways and that especially can isolate the particular process behind the model.

One transport model that has been proposed is the paleoclassical model.[3–5] The main idea of the paleoclassical model is that as current-induced poloidal magnetic flux diffuses out of the tokamak, it carries with it particles and heat. The model has been used to explain some experimentally observed phenomena, with some success.[6] To further test the paleoclassical transport model, in this work the transport equations are solved in the outer half of the edge pedestal assuming paleoclassical transport to be the only transport process there. This model is termed the Paleoclassical-Based Pedestal Model or PCBPM.

The layout of the paper is as follows. In section 2, the PCBPM is formalized by solving the transport equations for the electron density n_e and temperature T_e, with paleoclassical transport as the only transport process. The following section describes how the pedestal profiles are measured and characterized in DIII-D.[7] The predictions from the PCBPM are compared to measurements in section 4. The results are then discussed and summarized in the concluding sections.

2. THE PALEOCLASSICAL BASED PEDESTAL MODEL (PCBPM)

The flux surface averaged density and energy transport equations

$$\langle \nabla \cdot \mathbf{\Gamma} \rangle \equiv \frac{1}{V'} \frac{\mathrm{d}}{\mathrm{d}\rho} (V' \Gamma) = \langle S_n \rangle \tag{1}$$

$$\langle \nabla \cdot \mathbf{q} \rangle \equiv \frac{1}{V'} \frac{\mathrm{d}}{\mathrm{d}\rho} \left[V' \left(\Upsilon + \frac{5}{2} T \Gamma \right) \right] = Q^{net} \tag{2}$$

are the starting point of the paleoclassical based pedestal model. Here $\mathbf{\Gamma}$ and $\mathbf{q}$ are the particle and energy fluxes, respectively, with Γ and Υ the flux surface averaged fluxes; $\langle S_n \rangle$ and Q^{net} are the sources of particles and energy; T is the temperature; ρ is the radial coordinate, given as the square root of the toroidal flux, with a prime $'$ denoting $\mathrm{d}/\mathrm{d}\rho$; and V is the volume enclosed by the ρ surface. The paleoclassical particle density and heat fluxes are[5]

$$\Gamma^{\mathrm{pc}} = -\frac{1}{V'} \frac{\mathrm{d}}{\mathrm{d}\rho} \left(V' n_{\mathrm{e}} \bar{D}_\eta \right) \tag{3}$$

$$\langle \nabla \cdot \mathbf{q}^{\mathrm{pc}} \rangle = -\frac{M+1}{V'} \frac{\mathrm{d}^2}{\mathrm{d}\rho^2} \left(V' \bar{D}_\eta \frac{3}{2} n T \right), \tag{4}$$

and other forms of transport are assumed to be negligible in the pedestal. The primary paleoclassical parameter is the magnetic diffusivity

$$\bar{D}_\eta \equiv D_\eta a^2 / \bar{a}^2 \equiv \frac{\eta_\parallel}{\mu_0} \frac{a^2}{\bar{a}^2} \tag{5}$$

where $\eta_\parallel$ is the parallel neoclassical resistivity, μ_0 is the permittivity of free space, $a = \max(\rho)$ is the minor radius of the plasma, and $\bar{a}$ is a geometric factor. The term M in (4) is a helical winding factor for the electrons whose value $M \to 0$ as $\rho \to a$. (For ions $M = 0$ always.[5]) The complete form of M is given in Ref. 3.

By putting (3) and the electron version of (4) into (1) and (2), n_{e} and $\mathrm{d}T_{\mathrm{e}}/\mathrm{d}\rho \equiv \nabla T_{\mathrm{e}}$ can be solved for analytically as

$$n_{\mathrm{e}}^{\mathrm{pc}}(\rho) = \frac{n_{\mathrm{e}}(a) \bar{D}_\eta(a) V'(a) + \int_\rho^a \dot{N}_{\mathrm{e}} \mathrm{d}\rho}{\bar{D}_\eta(\rho) V'(\rho)} \tag{6}$$

$$-\frac{\mathrm{d}T_{\mathrm{e}}^{\mathrm{pc}}}{\mathrm{d}\rho} = \frac{P_{\mathrm{e}} - (3/2)\dot{N}_{\mathrm{e}} T_{\mathrm{e}}}{(3/2)(V' \bar{D}_\eta n_{\mathrm{e}})}. \tag{7}$$

This last equation can be integrated to yield

$$T_{\mathrm{e}}^{\mathrm{pc}} = T_{\mathrm{e}}(a) + \int_{\rho}^{a} \frac{P_{\mathrm{e}} - (3/2)\dot{N}_{\mathrm{e}} T_{\mathrm{e}}}{(3/2)(V' \bar{D}_{\eta} n_{\mathrm{e}})} \mathrm{d}\rho. \tag{8}$$

These equations will be evaluated at a particular value of $\rho = \rho_{\mathrm{REF}}$ in the pedestal.

A closer examination of the geometric factor

$$\bar{a} \equiv a \sqrt{\frac{\langle R^{-2} \rangle}{\langle |\nabla \rho|^2 / R^2 \rangle}}$$

reveals that the term in the denominator has a singularity at the separatrix of diverted plasmas. Therefore, a substitution

$$\bar{a}(\rho > \rho_{\mathrm{REF}}) \rightarrow \bar{a}(\rho_{\mathrm{REF}}) \tag{9}$$

is used in the evaluation of (7) and (8).

3. EXPERIMENTAL MEASUREMENTS

Predictions from the paleoclassical-based pedestal model will be compared to measurements taken during H-mode plasma shots on the DIII-D tokamak. The original database for comparisons was the PEDSCALE database compiled by Osborne.[8] Further comparisons have been made to shots from several experiments of the DIII-D 2011 campaign. Table 1 shows the wide range of the parameters of the shots for which the PCBPM has been evaluated.

In the DIII-D tokamak, n_e and T_e are measured using the Thomson scattering technique. Between the 2010 and 2011 campaigns, the Thomson system was upgraded[9] to have almost twice as many channels in the pedestal region. As well, several 50 Hz lasers were added to complement the existing 20 Hz lasers. The former allows more confidence in the gradients measured in the pedestal, especially in the steep gradient region. The latter allows for a shorter sampling time to ensure that a reasonable number of ELM phase specific time slices are being used. In addition, the newer 50 Hz lasers have a larger energy per pulse, which leads to a larger signal to noise ratio and presumably more accurate measurements. Because of this upgrade, the data are presented as being from the PEDSCALE database (pre-2011) or from the 2011 DIII-D run year.

The R, Z positions of the n_e and T_e data are converted to ρ space using an equilibrium mapping reconstructed at each Thomson laser pulse time. The data are binned according to ELM phase and then a particular subset (mostly 80–99% of the ELM phase) is fit to a modified tanh function

$$\mathrm{mtanh}(\rho) = \frac{c_2 - c_3}{2}\frac{(1 + c_4 z)e^z - e^{-z}}{e^z + e^{-z}} + \frac{c_2 + c_3}{2},$$

where $z \equiv 2(c_0 - \rho)/c_1$, and c_0 is the symmetry radius at the steepest part of the pedestal. (Further details on the experimental methods can be found in Ref. 10.) The value of c_0 for the T_e fit ($\equiv \rho_{_T}$) will be used for the reference radial location at which to evaluate the predictions of section 2.

When the data are fit with the mtanh, there are uncertainties associated with each of the fitting parameters. These uncertainties are propagated[11] through the paleoclassical calculations and thus provide the error bars on the PCBPM predictions of the following section.

Table 1. Ranges of parameters for the 158 DIII-D conditions considered in this work.

Parameter	Range	Mean	Median
a [m]	0.52–0.61	0.58	0.58
β_{N}	0.97–3.42	1.80	1.76
β_{p}	0.47–2.60	1.08	0.95
B_{T} [T]	0.98–2.14	2.00	2.10
δ_{l}	0.06–0.73	0.47	0.40
δ_{u}	0.04–0.84	0.28	0.24
I_{p} [MA]	0.46–1.50	1.01	1.00
κ	1.71–1.89	1.78	1.76
ℓ_{i}	0.70–1.19	0.96	0.97
ν_*^{ped}	0.09–2.81	0.96	0.88
Heating power [MW]	1.80–12.40	4.97	4.53
q_{95}	3.08–13.27	5.46	4.92
R_{magaxis} [m]	1.72–1.88	1.78	1.77
R_{out} [m]	2.22–2.31	2.28	2.28
Volume [m^3]	14.72–19.46	17.36	17.19

4. COMPARISON OF PREDICTIONS TO MEASUREMENT

4.1. Temperature Gradient

The first shots for this study against which comparisons were made of the paleoclassical pedestal model were those of the PEDSCALE database.[8] The ∇T_e predictions and measurements for this database are shown in figure 1. A majority of the points lie around equality; this can be quantified by looking at the mean ratio of $\nabla T_\mathrm{e}^\mathrm{pc}/\nabla T_\mathrm{e}^\mathrm{exp} = 1.1 \pm 0.6$, which is encouraging for the PCBPM. However, the linear correlation coefficient for the nominal values is -0.08. The furthest outliers (those marked 133137, 131499, and 136186) led to an investigation of why these points are so far off. It turns out that for 133137 and 131499, the electron effective conductive heat flow term P_e in (7) is uncharacteristically small — a factor of 10 smaller than the ion P_i for 133137 and even negative for 131499 — and is dominated by a large collisional energy exchange from electrons to ions. Small uncertainties in the measured difference between ion and electron temeratures could potentially lead to uncertainties in the exchange term, particularly at high density. To try to compensate for this possible systematic difference, the ion and electron versions of the energy transport equation (2) can be added so that the exchange terms mostly cancel. Then using only the paleoclassical transport of (4), the summed equation can be solved for ∇T_e to yield

$$-\frac{\mathrm{d}T_\mathrm{e}^\mathrm{pc}}{\mathrm{d}\rho} = \frac{(P_\mathrm{e}+P_\mathrm{i})/2 - \dfrac{3}{4}\dot{N}_\mathrm{e}(T_\mathrm{e}+n_\mathrm{i}T_\mathrm{i}/n_\mathrm{e})}{\dfrac{3}{2}V'\bar{D}_\eta n_\mathrm{e}} \frac{2}{1+(n_\mathrm{i}T_\mathrm{i}/n_\mathrm{e})'/T_\mathrm{e}'}. \tag{10}$$

The PCBPM predictions using (10) are shown as ▶ in figure 2 (mean ratio $\nabla T_\mathrm{e}^\mathrm{pc}/\nabla T_\mathrm{e}^\mathrm{exp} = 1.7 \pm 0.7$ with correlation=0.8), and are overlayed with the predictions using (7), shown as •. It is striking that with (10) nearly all of the points lie within error bars of equality or to the right of equality. This would indicate that paleoclassical transport by itself is predicting either the right amount of transport or too little, which is consistent with the hypothesis that paleoclassical transport produces a minimum level of transport. (If a gradient is overpredicted, that means the transport is underpredicted.)

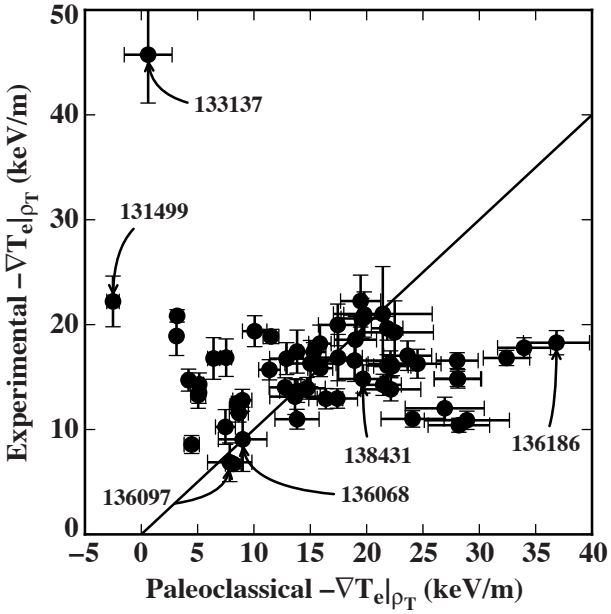

Figure 1. Experimentally measured ∇T_e versus the PCBPM predicted ∇T_e using (7) for shots from the PEDSCALE *database. The black solid line is equality.*

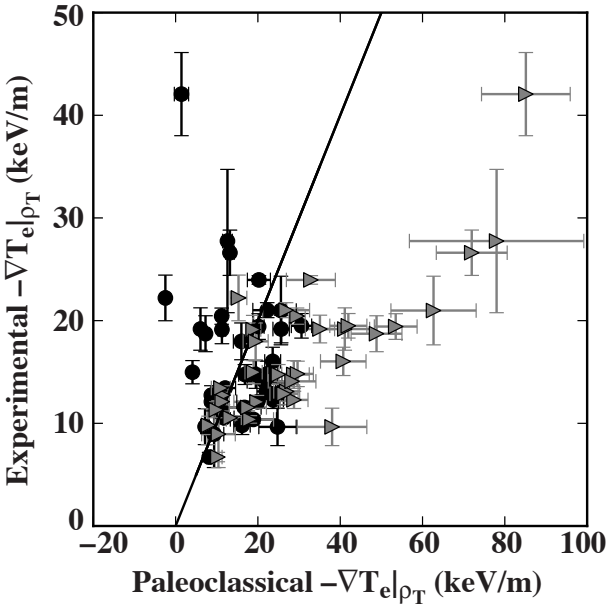

Figure 2. Experimentally measured ∇T_e versus the PCBPM predictions based on (7) (•) or (10) (▶) for shots from the PEDSCALE *database. The black solid line is equality. (Let it be noted that there are fewer points • here than in figure 1 because some of the database was lost when DIII-D suffered an MDS+ server failure.)*

The predictions for the shots from the DIII-D 2011 run campaign are shown in figure 3 overlaid with those from the original PEDSCALE database. One observation is that the range of measured temperature gradients has not been extended beyond

that observed previously in the database. (With the upgraded Thomson system, the increased radial resolution would be able to measure steeper gradients than before the upgrade.) Another observation is that the PCBPM gradient predictions are generally greater than or equal to the measured gradients (mean ratio $\nabla T_{\rm e}^{\rm pc}/\nabla T_{\rm e}^{\rm exp} = 1.7 \pm 1.1$ with correlation=0.55). This is still consistent with paleoclassical transport processes producing a minimum level of transport. For the largest overpredictions an additional energy transport channel would be necessary to properly model the pedestal.

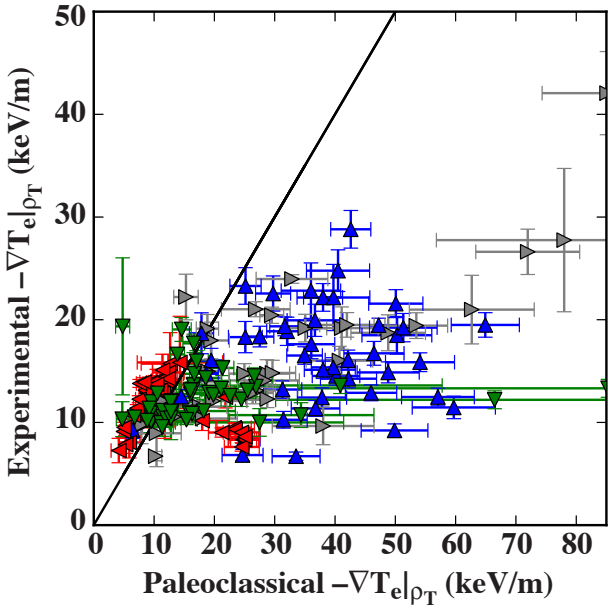

Figure 3. Experimentally measured $\nabla T_{\rm e}$ versus the PCBPM predicted $\nabla T_{\rm e}$ using (10). The different symbols denote different experiments from the 2011 run year (▼,▲,◀) or from the PEDSCALE *database (▶).*

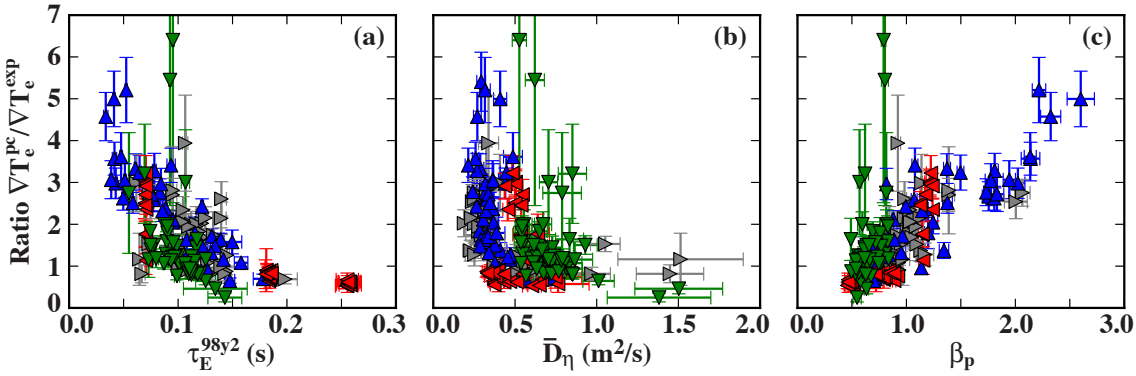

Figure 4. The ratio $\nabla T_{\rm e}^{\rm pc}/\nabla T_{\rm e}^{\rm exp}$ versus (a) the energy confinement time $\tau_{\rm E}^{\rm 98y2}$, (b) the magnetic diffusivity $\bar{D}_\eta$, and (c) the poloidal normalized pressure $\beta_{\rm p}$.

In order to understand and deconvolve the parametric dependencies of the predictions shown in figure 3, the ratio of prediction to measurement was plotted against several plasma parameters. The plots for the parameters judged to be most interesting are shown in figure 4. Here we see that the agreement (ratio=1) between prediction and measurement is best for larger confinement times ($\tau_{\rm E}^{\rm 98y2}$ is the empirical scaling of energy confinement time as defined in Ref. 12). This is consistent with paleoclassical processes producing a minimum level of transport: at smaller confinement times, there must be additional transport processes active to degrade confinement, and at higher confinement times, these additional processes are subdued such that paleoclassical processes are dominant. From figure 4(b), we see that while agreement between prediction and measurement is better for larger values of the magnetic diffusivity $\bar{D}_\eta$, the correlation is not as strong as $\tau_{\rm E}^{\rm 98y2}$. Finally, the ratio increaes linearly with $\beta_{\rm p}$, and agreement is best at lower $\beta_{\rm p}$. It is interesting to note that it was found previously[13] that empirically the width of the pedestal in DIII-D scales as $\beta_{\rm p}^{1/2}$. The EPED1.6 model obtains a similar scaling for the pedestal width by invoking Kinetic Ballooning Mode (KBM) constraints on the pedestal.[2] Further work needs to be done to determine if the KBM provides the additional transport that is missing when the PCBPM overpredicts the gradients at higher $\beta_{\rm p}$ and lower $\tau_{\rm E}^{\rm 98y2}$.

4.2. Density

Unlike the PCBPM temperature gradient predictions, which were fairly close to measurements, the original electron density predictions from (6) for the PEDSCALE database were $\sim 5\times$ too large and are shown as $\bullet$ in figure 5. However, once the singular nature of the $\bar{a}$ factor is taken into account, shown as $\blacktriangleright$ in figure 5, the density is only overpredicted by a factor of ~ 2.

The PCBPM density predictions using (9) for shots from the 2011 run year are plotted ($\blacktriangledown$,$\blacktriangleleft$,$\blacktriangle$) with the PEDSCALE results ($\blacktriangleright$) in figure 6. Overall the mean ratio is $n_{\rm e}^{\rm pc}/n_{\rm e}^{\rm exp} = 2.1 \pm 0.7$ with a correlation of 0.89.

The neutral fuelling model that is being used is a simple model that does not account for 2D effects. However, the neutral fuelling is not a large part of the PCBPM predictions: if $\dot{N}_e$ is set to 0, the mean ratio $n_{\rm e}^{\rm pc}/n_{\rm e}^{\rm exp}$ decreases only a small amount to 2.0 ± 0.6.

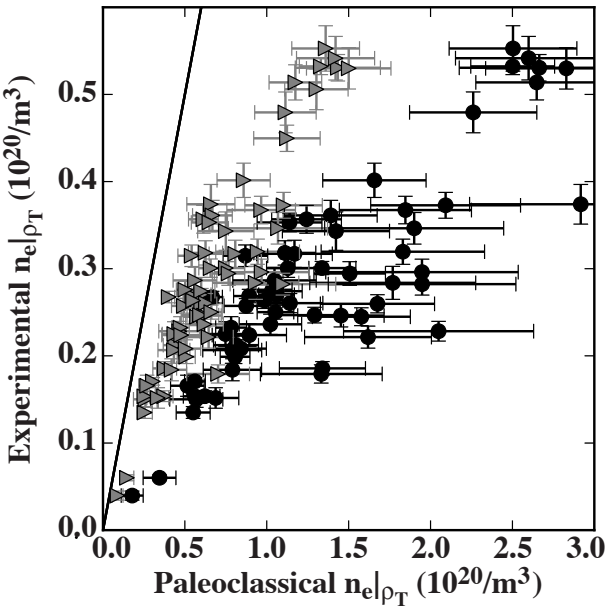

Figure 5. Experimentally measured n_e versus the PCBPM prediction for shots from the PEDSCALE *database. The different points are evaluated using (6) (•) or (9) (►).*

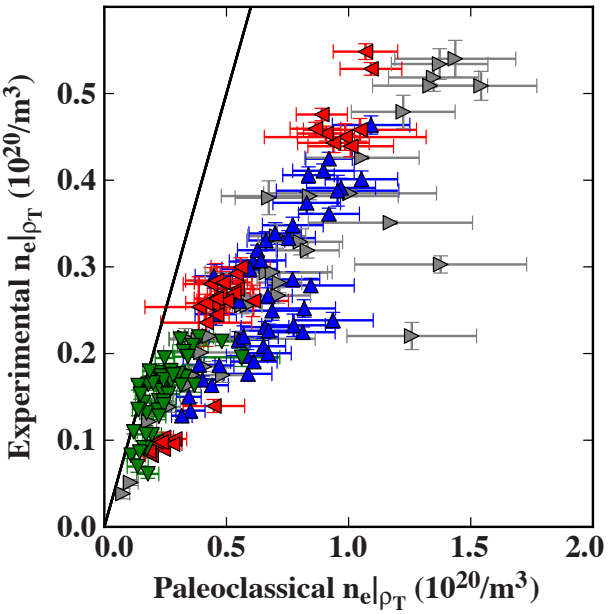

Figure 6. Experimentally measured n_e versus the PCBPM prediction using (9) for shots from the 2011 run year (▼,◄,▲) and from the PEDSCALE *database (►).*

5. DISCUSSION

The results of the previous section are not inconsistent with paleoclassical processes producing the minimum level of transport. Further work must be done to show whether there is significant fluctuation induced transport, ion orbit loss transport, or even neoclassical transport that will bring the transport up to apparent experimental levels. Whatever the additional transport, more particle transport than thermal transport is needed to account for differences between the density and temperature predictions.

Up to this point, the PCBPM predictions are done interpretively, i.e. experimental profiles are used in the calculation of D_η, and a power balance analysis is necessary to establish the sources S and Q. A further refinement is to use the profiles from a given iteration in the next iteration, until a steady state is reached. Steady states are achievable for each of the cases shown; however, the results are not significantly different.

6. SUMMARY

A model for the electron density and temperature pedestal structures was presented, based on paleoclassical processes providing the dominant transport. The model was used to predict the electron density and temperature gradient in the steep gradient region of the edge pedestal for a variety of DIII-D shots. These predictions compare favorably with measurements, in particular that the paleoclassical processes produce the minimum level of transport. Additional transport is apparently needed at high β_{p} and low $\tau_{\mathrm{E}}^{98\mathrm{y}2}$ in order to produce a higher fidelity model of the pedestal.

ACKNOWLEDGMENT

This work is supported in part by the U.S. Department of Energy under DE-FC02-04ER54698 and DE-FG02-92ER54139.

REFERENCES

[1] J. E. Kinsey, G. M. Staebler, J. Candy, R. E. Waltz, and R. V. Budny. ITER predictions using the GYRO verified and experimentally validated trapped gyro-Landau fluid transport model. Nucl. Fusion **51**(8), 083001 (2011).

[2] P. B. Snyder, R. J. Groebner, A. W. Leonard, T. H. Osborne, and H. R. Wilson. Development and validation of a predictive model for the pedestal height. Phys. Plasmas **16**(5), 056118 (2009).

[3] J. D. Callen. Paleoclassical transport in low-collisionality toroidal plasmas. Phys. Plasmas **12**(9), 092512 (2005).

[4] J. D. Callen, J. M. Canik, and S. P. Smith. Pedestal Structure Model. Technical Report CPTC 11-3, U. Wisc. (submitted to Phys. Rev. Lett.).

[5] J. D. Callen. Model for pedestal structure. Technical Report CPTC 11-4, U. Wisc. (submitted to Phys. Plasmas).

[6] J. D. Callen, J. K. Anderson, T. C. Arlen, G. Bateman, R. V. Budny, T. Fujita, C. M. Greenfield, M. Greenwald, R. J. Groebner, D. N. Hill, G. M. D. Hogeweij, S. M. Kaye, A. H. Kritz, E. A. Lazarus, A. C. Leonard, M. A. Mahdavi, H. S. McLean, T. H. Osborne, A. Y. Pankin, C. C. Petty, J. S. Sarff, H. E. St John, W. M. Stacey, D. Stutman, E. J. Synakowski, and K. Tritz. Experimental tests of paleoclassical transport. Nucl. Fusion **47**(11), 1449 (2007).

[7] J. L. Luxon. A design retrospective of the DIII-D tokamak. Nucl. Fusion **42**(5), 614 (2002).

[8] T. H. Osborne, M. N. A Beurskens, J. D. Callen, L. Frassinetti, R. J. Groebner, J. W. Hughes, S. Saarelma, P. A. Schneider, S. P. Smith, P. B. Snyder, E. Wolfrumand and Z. Yan. Scaling of H-mode Pedestal and ELM Characteristics from a Multi-Tokamak Database and Comparison to Theoretical Models. 13th International H-mode Workshop, 2011.

[9] D. Eldon, B. D. Bray, T. M. Deterly, C. Liu, D. M. Ponce, M. Watkins, R. J. Groebner, A. W. Leonard, T. H. Osborne, P. B. Snyder, R. L. Boivin, and G. R. Tynan. Initial results of the high resolution edge Thomson Scattering upgrade at DIII-D. 13th International H-mode Workshop, 2011.

[10] T. H. Osborne, P. B. Snyder, K. H. Burrell, T. E. Evans, M. E. Fenstermacher, A. W. Leonard, R. A. Moyer, M. J. Schaffer, and W. P. West. Edge stability of stationary ELM-suppressed regimes on DIII-D. Journal of Physics: Conference Series, **123**(1), 012014 (2008).

[11] Eric O. Lebigot. Uncertainties: a Python package for calculations with uncertainties.

[12] ITER Physics Expert Group on Confinement, Transport, ITER Physics Expert Group on Confinement Modelling, Database, and ITER Physics Basis Editors. Chapter2: Plasma confinement and transport. Nucl. Fusion **39**(12), 2175 (1999).

[13] T. H. Osborne, K. H. Burrell, R. J. Groebner, L. L. Lao, A. W. Leonard, R. Maingi, R. L. Miller, G. D. Porter, G. M. Staebler, and A. D. Turnbull. H-mode pedestal characteristics in ITER shape discharges on DIII-D. J. Nucl. Mater. **266-269**, 131 (1999).